Solis Clear Sky Scheme: Extension to High Turbidity, Development and Validation

Pierre Ineichen

University of Geneva, Institute for Environmental Sciences,
Department F.-A. Forel for environmental and aquatic sciences

Abstract

The Solis clear sky model is a spectral scheme based on radiative transfer calculations and the Lambert–Beer relation. Its broadband version is a simplified fast analytical version; it is limited to broadband aerosol optical depths at 700nm lower than 0.45, which is a weakness when applied in countries with very high turbidity such as China or India. This paper aims to extend the validity of the model to higher aerosol optical depth values. In 2014, Zhang published a modification of the scheme to extend its validity to aerosol optical depth values up to 6.5, but this extension is only applicable for the beam irradiance component and presents some weakness for very high turbidity values. In a first step, we tried to apply a correction to the Zhang adaptation. In order to extend the use of the original simplified version of Solis for high turbidity, we developed a new version of the broadband Solis, valid for the three components, global, beam and diffuse, and for the four aerosol types defined by Shettle and Fenn.

Keywords: Solis scheme, clear sky, radiation model, radiative transfer, high turbidity, water vapor

1. Introduction

The clear sky Solis scheme was first developed within the Mesor European program whose subject was the *management and exploitation of solar resource knowledge*. In 2008, Ineichen published a broadband analytical version of the Solis model for rural aerosol type, and in 2010 a version in the form of an excel tool for the four types of aerosols as defined by Shettle and Fenn. These versions were limited to aerosol optical depth values aod_{700} lower than 0.45. The anthropogenic heating and transportation activities conducted to a serious increase of the turbidity in countries like India or China. Looking into the limitations of the state of the art clear sky models, it appears that none is applicable for high turbidity. Indeed, for example, Gueymard CPCR2 model (Gueymard 1989) is limited to β turbidity values lower than 0.4 (which correspond to an aod_{700} of 0.64 for rural aerosol type, α = 1.3), Gueymard REST2 (Gueymard 2003) is limited to β = 1 (aod_{700} = 1.6, rural aerosol), Bird's model (Bird 1980) is defined for visibility values up to 23 km (which corresponds to an aod = 0.27) and the ESRA clear sky scheme (ESRA 2000, Rigollier 2000, Geiger 2002) was developed for Linke turbidity values T_L not exceeding a value of 7 (i.e. an aerosol optical depth aod_{700} = 0.44 for a 2 cm water vapor column). As the 2003 and 2008 versions of Solis diverge for high turbidity as shown by Zhang (2014), an extension of the model for higher turbidity values is needed.

This paper presents a validation and an adaptation of the model for the beam component extended by Zhang, and the development and validation of a new version of the analytical Solis scheme valid for the three radiation components, the global, the beam and the diffuse, and the four aerosol types, urban, rural, maritime and tropospheric.

2. The Solis scheme

The Solis scheme (Mueller 2004) is a model based on LibRadTran radiative transfer calculations (Mayer 2005, 2010). The basis of the model is the Lambert-Beer attenuation relation:

Selection and/or peer review under responsibility of Scientific Committee
doi:10.18086/swc.2017.23.02 Available at http://proceedings.ises.org

$$I_{bn} = I_o \cdot \exp(-M \cdot \tau) \qquad \text{(eq. 1)}$$

where I_o is the extraterrestrial irradiance, I_{bn} the normal beam irradiance reaching the ground, M the optical air mass and τ the total atmospheric optical depth. This expression of the atmospheric transmittance is valid for monochromatic radiation, and the optical depth is then constant over the air mass range. Due to the non-linear nature of the exponential function, the Lambert-Beer relation has to be modified to extend the expression to wavelength bands; it takes then the following form:

$$I_{bn} = I_o \cdot \exp\left(-\frac{\tau}{\sin^b h}\right) \qquad \text{(eq. 2)}$$

where h is the solar elevation angle and b the fitting parameter obtained from RTM calculations at two different solar elevation angles.

When dealing with global irradiance, the Lambert-Beer relation is no longer applicable because of the back scatter effects, but remains a relatively good approximation, and

$$I_{gh} = I_o \cdot \exp\left(-\frac{\tau}{\sin^g h}\right) \cdot \sin h \qquad \text{(eq. 3)}$$

is a good fitting function for the horizontal global irradiance (Mueller 2004).

The source of the incoming diffuse irradiance is the attenuation of the beam radiation due to scattering process and it cannot be described in term of attenuation of the incoming radiation. Nevertheless, skipping the sin h term, the modified Lambert-Beer relation also works well:

$$I_{dh} = I_o \cdot \exp\left(-\frac{\tau}{\sin^d h}\right) \qquad \text{(eq. 4)}$$

At high aerosol load, *Io* has to be enhanced for the global and diffuse irradiance calculations, and a common modified *Io'* irradiance is defined for the three radiation components. The final expression of the model has then the following form:

$$I_{bn} = I'_o \cdot \exp\left(-\frac{\tau_b}{\sin^b h}\right) \quad I_{gh} = I'_o \cdot \exp\left(-\frac{\tau_g}{\sin^g h}\right) \cdot \sin h \quad I_{dh} = I'_o \cdot \exp\left(-\frac{\tau_d}{\sin^d h}\right) \qquad \text{(eq. 5)}$$

where τ_b, τ_g and τ_d are respectively the beam, global and diffuse total optical depths, and b, g and d the corresponding fitting parameters obtained from RTM calculations.

3. Zhang extension validation

To extend the range of the model application, Zhang added two terms in the extinction equation for the beam component, one for the aerosol optical depth K_{aod} , and one for the water vapor column K_w. These two terms are constant and defined in order to have a smooth behavior at aod_{700} = 0.45 which is the original Solis *aod* limitation (i.e. a null derivative for aod_{700} = 0.45).

We made a validation of the extended model against data evaluated with the Radiative Transfer Model (RTM) LibRadTran for a wide range of aerosol optical depths values, water vapor column and altitudes. As the Zhang extension shows slight deviations for low water vapor column and high turbidity values when plotting the modeled beam irradiance against the correspondent value calculated with the help of the LibRadTran radiation transfer model (see Fig. 1, left), we adapted the Zhang extension coefficient K_{aod} by making it *aod* dependent. This allowed to slightly better aligning the dots on the 1:1 diagonal as illustrated on the right graph of Fig. 1.

For altitudes from sea level to 7000 m, water vapor from 0.05 cm to 10 cm and *aod* from 0 to 7, and a solar elevation of 60°, the results are the following:

- Zhang extension *mbd* = 0.2% *sd* = 4.7%
- Zhang + Ineichen *mbd* = 0.2% *sd* = 2.8%.

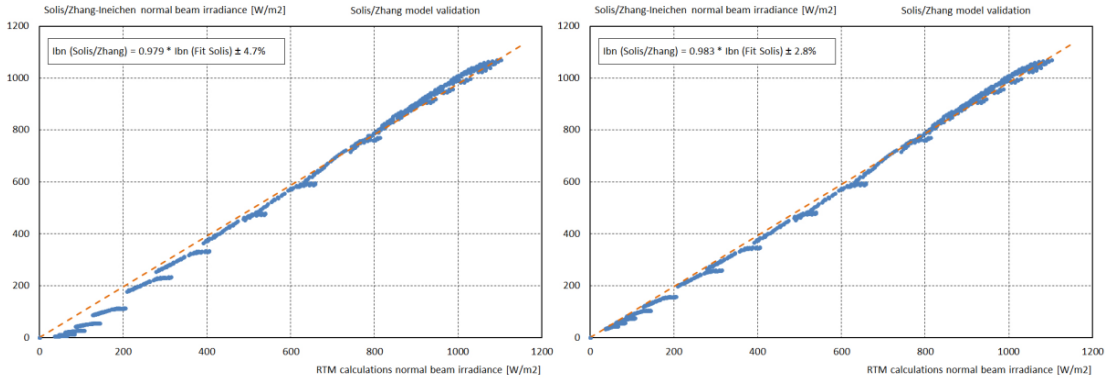

Fig. 1: Normal beam validation for the Zhang extension (left) and the Zhang-Ineichen correction (right)

4. Solis extension to high turbidity

The weakness of the Zhang extension is that it derives only the beam component. To circumvent this problem, we developed a Solis-2017 version that is applicable for values of *aod* up to 7. This means that the model goes up to very high atmospheric aerosol load, but one has to keep in mind that above *aod* = 2, it is not clear that the turbidity can be considered as an aerosol optical depth, but a turbidity due to bigger particles like sand, or in our countries, high altitude thin clouds. Nevertheless, it is important that in on-line automatic production processes, the model does not diverge and still derive coherent values, even with some discrepancies with ground measurements.

4.1. Model development

In a first step, we made spectral calculations with LibRadTran for the following parameters:

Tab. 1: aerosol types, altitudes, optical depths and water vapor columns values for the RTM calculations

aerosol type	altitude	aod_{550}	w [cm]
urban	sea level	0.01	0.01
rural	500m	0.03	0.03
maritime	1000m	0.05	0.05
tropospheric	2000m	0.1	1
	3000m	0.15	0.15
	4000m	0.2	0.2
	5000m	0.4	0.3
	6000m	0.7	0.5
	7000m	1	1
		1.5	1.5
		2	2
		3	3
		4	4
		5	6
		6	8
		7	10

These RTM calculations permit to generate the seven coefficients that drive the model: I_o', τ_b, b, τ_g, g, τ_d, and d. The next step is to develop an analytical formulation for these coefficients with the 4 input parameters given in Tab. 1.

The analysis of I_o', τ_b, and τ_g shows a similar behavior for these three parameters. The first analyzed dependence is with the aerosols optical depth *aod*. A third order polynomial model is applicable for the three parameters of the form:

$$I_o'/I_o = a \cdot aod^3 + b \cdot aod^2 + c \cdot aod + d \quad \text{(eq. 6)}$$

The behavior for I_o' and τ are represented on the Fig. 2 below.

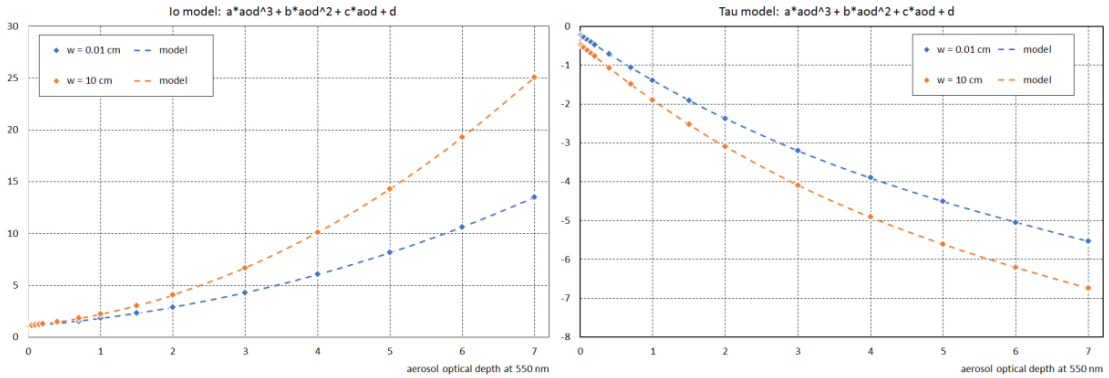

Fig. 2: Normal beam validation for the Zhang extension (left) and the Zhang-Ineichen correction (right)

We then analyzed the dependence of each of the a, b, c and d coefficient of equation 6 with the atmospheric water vapor content. The behavior of the four coefficients shows a water vapor dependence of the form:

$$n = n1 \cdot w^{0.5} + n2 \cdot \ln(w) + n3 \quad \text{(eq. 7)}$$

The best fits of two of these coefficients are given on the Fig. 3

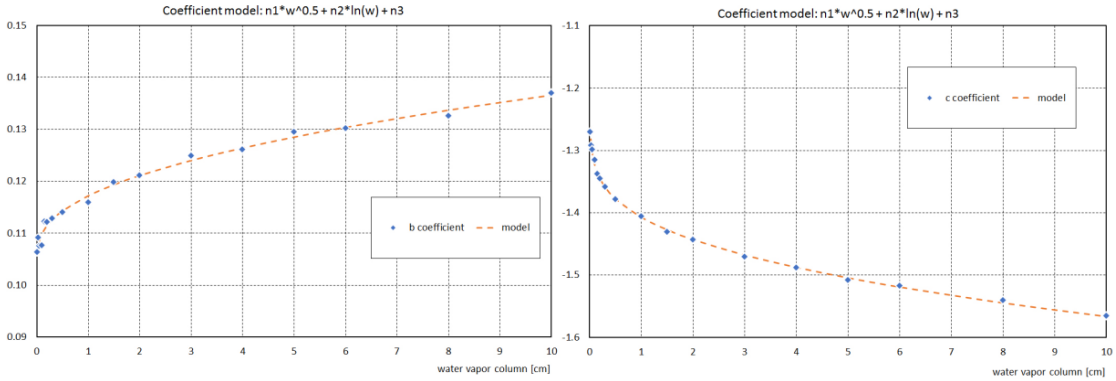

Fig. 3: Behavior of two of the cubic equation coefficients with the water vapor column

Finally, the dependence of the three above coefficients with the altitude, respectively the normalized atmospheric pressure p/p_o (the pressure p at a given altitude normalized by the corresponding sea level pressure p_o) is analyzed. It appears that a linear regression gives the best results.

The model has then the following form:

$$a = a_1 \cdot w^{0.5} + a_2 \cdot \ln(w) + a_3 \quad \text{(eq. 7a)}$$
$$b = b_1 \cdot w^{0.5} + b_2 \cdot \ln(w) + b_3 \quad \text{(eq. 7b)}$$
$$c = c_1 \cdot w^{0.5} + c_2 \cdot \ln(w) + c_3 \quad \text{(eq. 7c)}$$
$$d = d_1 \cdot w^{0.5} + d_2 \cdot \ln(w) + d_3 \quad \text{(eq. 7d)}$$

and each of the n_i coefficient is obtained with a linear function of p/p_o

$$n_i = n_{i1} \cdot p/p_o + n_{i2} \quad \text{(eq. 8)}$$

Finally, the inputs for the model for I_o', τ_b and τ_g, consist of the aerosol optical depth at 550 nm aod_{550}, the water vapor content of the atmosphere w and the relative atmospheric pressure p/p_o. The corresponding coefficient are given in a 3x3x2 matrix.

For τ_d, the best correlation we found is a relation with to τ_b and τ_g that has the form:

$$\tau_d = e + f \cdot \tau_g + g / \tau_b + h / \tau_g^{\,2} + i \cdot \tau_g / \tau_b \quad \text{(eq. 9)}$$

The exponents of the sin (h) in the Lambert-Beer function are respectively best fitted as follow:

$$g = c_{a1} + c_{a2} \cdot \ln(w) + c_{a3} \cdot \ln(aod) + c_{a4} \cdot \ln(w)^2 + c_{a5} \cdot \ln(aod)^2 + c_{a6} \cdot \ln(w) \cdot \ln(aod) \qquad \text{(eq. 10)}$$

$$b = c_{b1} \cdot w^{\,cb2} \cdot c_{b3}^{\,aod} \qquad \text{(eq.11)}$$

$$d = c_{d1} + c_{d2} \cdot \ln(w) + c_{d3} \cdot aod + c_{d4} \cdot aod^2 + c_{d5} \cdot aod^3 + c_{d6} \cdot aod^4 + c_{d7} \cdot aod^5 \qquad \text{(eq. 12)}$$

4.2 Parameter validation

The validation of the seven parameters of the model is expressed as scatter plots between the modeled parameter and the corresponding LibRadTran calculated parameter. The validation points should be aligned on the 1:1 diagonal. On the graphs are also given the average parameter value, the mean bias difference *mbd*, the standard deviation *sd* and the correlation coefficient R^2. An illustration is given on Fig. 4 for I_o' and the *a* coefficient, urban aerosol type.

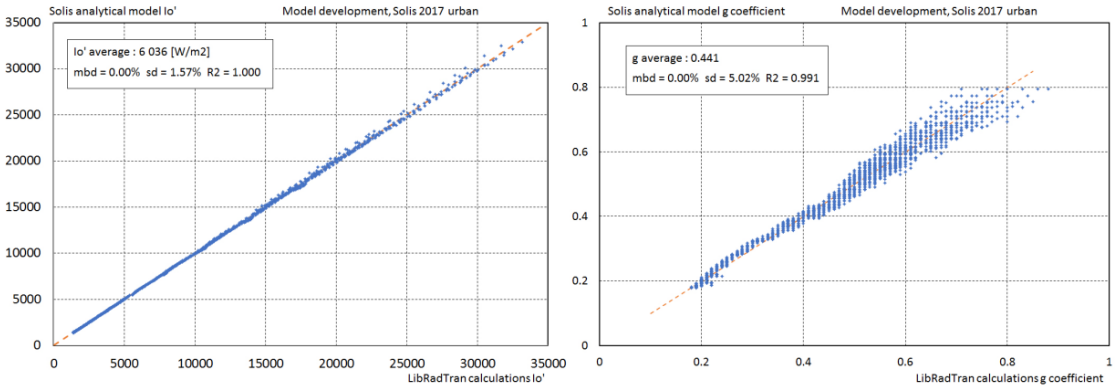

Fig. 4: I_o' and *g* coefficient validation

The average, *mbd* and *sd* values cannot be taken as an absolute validation of the precision as all the values calculated from the input matrix (altitude, *aod* and *w)* have the same weight. Nevertheless, it gives a good idea of the roughness of the parameter best fit. These values are given in Tab. 2.

Tab. 2: Average, *mbd*, *sd* and R^2 for the I_o', τ_b, *b*, τ_g, *g*, τ_d, and *d* model.

	Io'				τ_g				*a*			
aerosol type	average	mbd	sd	R2	average	mbd	sd	R2	average	mbd	sd	R2
rural	6284	-0.5	92.9	1.000	-1.49	0.00	0.01	1.000	0.41	0.00	0.02	0.993
urban	6036	0.0	94.7	1.000	-1.68	0.00	0.02	1.000	0.44	0.00	0.02	0.991
tropo	12210	-7.8	133.9	1.000	-1.69	0.00	0.01	1.000	0.39	0.00	0.02	0.994
maritime	5380	0.2	40.3	1.000	-1.40	0.00	0.01	1.000	0.41	0.00	0.02	0.992
					τ_b				*b*			
rural					-2.21	0.00	0.01	1.000	0.42	0.00	0.02	0.965
urban					-2.21	0.00	0.01	1.000	0.44	0.00	0.03	0.941
tropo					-2.68	0.00	0.01	1.000	0.45	0.00	0.02	0.912
maritime					-2.08	0.00	0.01	1.000	0.40	0.00	0.02	0.976
					τ_d				*c*			
rural					-2.75	0.01	0.04	0.998	0.32	0.00	0.01	0.995
urban					-3.08	0.01	0.05	0.999	0.29	0.00	0.01	0.995
tropo					-2.86	0.01	0.04	0.999	0.31	0.00	0.01	0.995
maritime					-2.67	0.01	0.04	0.998	0.33	0.00	0.01	0.995

4.3 Irradiance validation

In the same way, the validation of the irradiance components is expressed as scatter plots and the usual first order statistics. Here again, due to the unweighted input matrix, the validation values obtained give not an absolute precision of the model. The scatter plots given on Fig. 5 below illustrate the behavior of the model. They represent the modeled values plotted against the corresponding values evaluated from RTM calculations, urban type aerosols, for the three components.

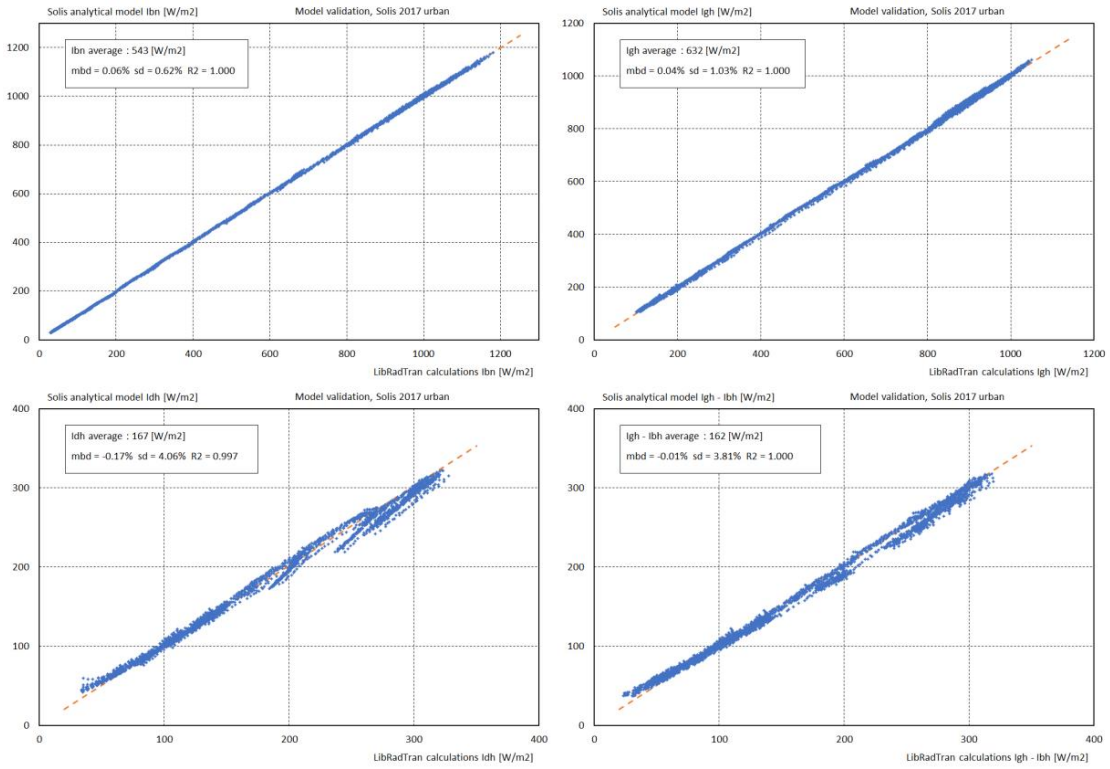

Fig. 5 Irradiance model validation

To obtain the diffuse component, there are two possibilities: the use of the model coefficients τ_d and d, or to evaluate it from the global and the beam components with the use of the closure equation $I_{dh} = I_{gh} - I_{gh}$. The diffuse obtained from the closure equation looks slightly better on Fig. 5, but it presents negative values for very low solar elevations.

The corresponding values are given in Tab. 3

Tab. 3: Average, *mbd*, *sd* and R^2 for the irradiance components.

	I_{gh}				I_{bn}				I_{dh}			
aerosol type	average	mbd	sd	R2	average	mbd	sd	R2	average	mbd	sd	R2
rural	727	0.4	3.9	1.000	549	0.0	4.7	1.000	223	0.5	7.3	0.998
urban	632	0.3	6.5	1.000	543	0.3	3.4	1.000	167	-0.3	6.8	0.997
tropo	740	0.2	4.7	1.000	559	-0.3	6.8	1.000	227	0.4	6.6	0.999
maritime	753	-1.3	16.7	0.997	519	-3.0	17.7	0.999	266	1.6	10.7	0.998

All the development and validation graphs for the urban aerosol type are given in the annex.

4.4 Components coherence

To visualize the behavior of the model and the coherence between the irradiance components, the model trends are represented for four typical values of aerosols optical depths *aod* (0.5, 0.9, 1.5 and 6) and a value of w = 1cm for the atmospheric water vapor column on Fig. 6. The ozone amount is taken constant at a value of 340 Dobson units, the aerosol characteristics is of urban type, and the albedo coefficient at 20%. On the left graph, the diffuse fraction I_{dh} / I_{gh} is represented versus the global clearness index K_t ($Kt = I_{gh} / I_o \sin h$), and on the right graph, the beam clearness index K_b ($K_b = I_{bn} / I_o$) versus the global clearness index. The Linke turbidity values T_L, evaluated from the aerosol optical depth and the water vapor column are also indicated on the graphs.

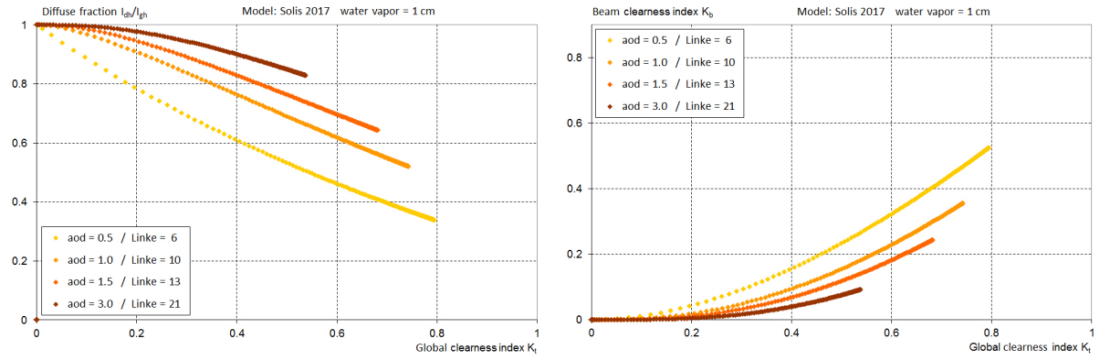

Fig. 6 Trends for the diffuse fraction and the beam clearness index versus the global clearness index

4.5 Validation on ground data from Geneva and Jaipur

The model should be validated against ground measurements acquired in highly polluted conditions. At this time, we had no access to such data (ground irradiances and *aod*); therefore, a preliminary validation is done on data acquired in Geneva for the years 2004 to 2011 where the *aod* is pretty low, and Jaipur with *aod* values up to 2.5 for 17 months in 2016 and 2017.

The average aerosol optical depth in Geneva is of order of 0.17 with a maximum of 0.5 during polluted episodes. As no specific aerosol optical depth values are measured in Geneva, we used one of the best state of the art model, REST2 (Gueymard 2004), to retrieve by retrofit the *aod* following the method described in Ineichen (2016). The clear sky condition selection is also described in Ineichen (2016). The results, illustrated on Fig. 7, are slightly better than for Solis 2008 (Ineichen 2016).

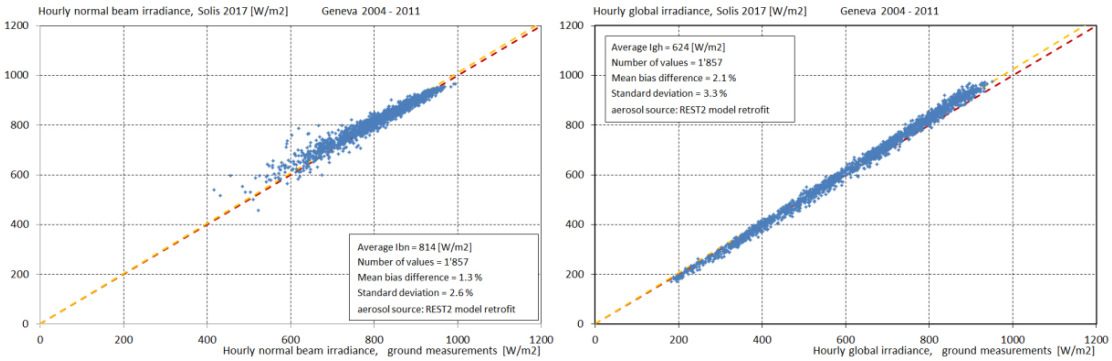

Fig. 7 Validation against ground data acquired in Geneva. The *aod* is retrofitted with REST2

For Jaipur, the aod_{550} values can reach 2.5, as this exceeds the REST2 limitations, we obtained values by retrofit with the use of Molineaux *bmpi* model (1998). The graphs are given on Fig. 8.

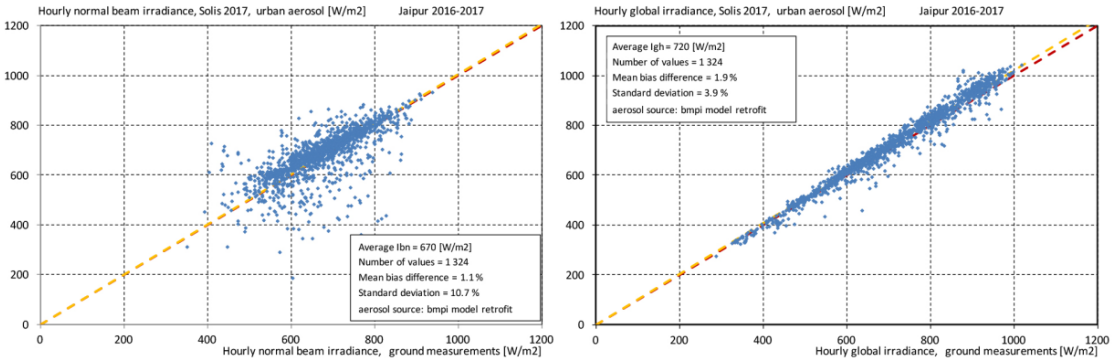

Fig. 8 Validation against ground data acquired in Jaipur. The *aod* is retrofitted with *bmpi* model.

It can be seen that the dispersion is higher, especially for the beam irradiance. This is due to the higher turbidity values, conditions for which it is difficult to determine the aerosol type. The extinction of the beam

irradiance can also be due to high altitude thin clouds or variability in the atmospheric water vapor column (evaluated from ground temperature and humidity).

5. Conclusion

When dealing with satellite images to derive the irradiance components on a wide space scale and every 15 minutes, the computer time should be as short as possible. The analytical Solis clear sky scheme was developed to fulfill this requirement but had the weakness to be limited to aerosol optical depth values lower than 0.45. The new analytical Solis scheme is valid for *aod* up to seven, even if very high values are not realistic as an optical depth; it is probably more due to bigger particles like sand, or in our countries, thin high altitude clouds. Nevertheless, in contrary to other clear sky models, this permit to produce coherent irradiance values, even with questionable input values.

The new Solis clear sky scheme is valid for aerosol optical depths values aod_{550} from 0.02 to 7, atmospheric water vapor w content from 0.01 to 10 cm, and altitude from sea level to 7000 m, and four aerosol types as defined by Shettle and Fenn. For the urban, rural and tropospheric aerosol types, the validation against the original RTM calculations presents no bias and a standard deviation lower than 1% for the global and the beam component, and 3% for the diffuse. When dealing with maritime aerosol type, the standard deviation is respectively 2.2%, 3.4% and 4% for the global, the beam and the diffuse components.

A preliminary validation against ground measurements acquired in Geneva and Jaipur gives a mean bias difference of 2%, a standard deviation of 3-4% for the global component, and a mean bias difference of 1.3% with a standard deviation of 2.6% and 10.7% for the beam component for respectively Geneva and Jaipur.

6. Nomenclature

I_{gh}	horizontal global irradiance	aod	aerosol optical depth
I_{bn}	normal beam irradiance	τ	total atmospheric optical depth
I_{dh}	horizontal diffuse irradiance	w	atmospheric water vapor column
I_o	sun-earth distance corrected solar constant	α	particle size exponent
K_t	global clearness index	β	turbidity coefficient
K_b	beam clearness index		
mbd	mean bias difference	M	optical air mass
sd	standart deviation	T_L	Linke turbidity
R^2	correlation coefficient	p	atmospheric pressure at the considered altitude
h	solar elevation	p_o	atmospheric pressure at sea level

7. References

ESRA, European Solar Radiation Atlas, 2000. Fourth edition, includ. CD-ROM. Edited by Greif J., Scharmer K.. Scientific advisors: Dogniaux R., Page J.K.. Authors: Wald L., Albuisson M., Czeplak G., Bourges B., Aguiar R., Lund H., Joukoff A., Terzenbach U., Beyer H.G., Borisenko E.P. Published for the Commission of the European Communities by Presses de l'Ecole, Ecole des Mines de Paris, France, France.

Geiger M., Diabaté L., Ménard L., Wald L., 2002. A web Service for Controlling the Quality of Measurements of Global Solar Irradiation. Solar Energy, 73 (6), 475-480.

Gueymard C., 1989. A two-band model for the calculation of clear Sky Solar Irradiance, Illuminance, and Photosynthetically Active Radiation at the Earth Surface. Solar Energy, Vol. 43, N° 5, 253-265

Gueymard C., 2003. Direct solar transmittance and irradiance predictions with broadband models. Part 1: Detailed theoretical performance assessment. Solar Energy 74, 355–379, Corrigendum: Solar Energy 76, 513.

Ineichen P., 2008. A broadband simplified version of the Solis clear sky model, Solar Energy, 82, 768-772. < http://archive-ouverte.unige.ch/unige:17186>

Ineichen P., 2010. A broadband simplified version of the Solis clear sky model, Excel tool. Available from: <http://www.unige.ch/energie/fr/equipe/ineichen/solis-tool/> (last access in Sept. 2017)

Ineichen P., 2016. Validation of models that estimate the clear sky global and beam solar irradiance. Solar Energy 132, 332–344 < http://archive-ouverte.unige.ch/unige:81856>

Mayer B. and Kylling A., 2005. Technical note: The LibRadTran software package for radiative transfer calculations – description and examples of use, Atmos. Chem. Phys., 5, 1855–1877, doi:10.5194/acp-5-1855-2005.

Mayer B., Kylling A., Emde C., Buras R., Hamann U., 2010. LibRadTran: library for radiative transfer calculations, Edition 1.0 for libRadtran version 1.5-beta, http://www.libradtran.org (last access in Sept. 2017).

Molineaux B., Ineichen P., O'Neill N., 1998. Equivalence of pyrheliometric and monochromatic aerosol optical depths at a single key wavelength. Applied Optics / Vol. 37, No. 30 < http://archive-ouverte.unige.ch/unige:17210>

Mueller R.W, Dagestad K.F., Ineichen P., Schroedter-Homscheidt M., Cros S., Dumortier D., Kuhlemann R., Olseth J.A., Piernavieja G., Reise C., Wald L., Heinemann D. 2004. Rethinking satellite based solar irradiance modelling - The SOLIS clear-sky module. Remote Sens. Environ. 91, 160-174

Rigollier C., Bauer O., Wald L., 2000. On the Clear Sky Model of the ESRA - European Solar Radiation Atlas - with Respect to the Heliosat Method. Solar Energy 68 (1), 33-48.

Shettle E.P, Fenn R.W., 1979. Models fort the aerosol of lower atmosphere and the effect of humidity variations on their optical properties.

Shettle E.P., 1989. Models of aerosols, clouds and precipitation for atmospheric propagation studies. AGARD Conference proceedings, Copenhagen, Denmark, 9-13 October

Zhang T., Stackhouse P.W., Chandler W.S., Westberg D.J., 2014. Application of a global-to-beam irradiance model to the NASA GEWEX SRB dataset: An extension of the NASA Surface meteorology and Solar Energy datasets. Solar Energy 110, 117–131

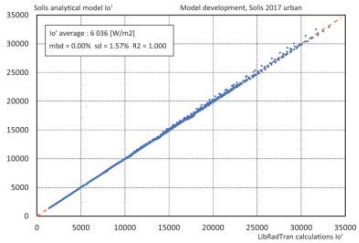

Annex

Development of the Solis 2017 model
Validation graphs and coefficients dependence for the urban type aerosol

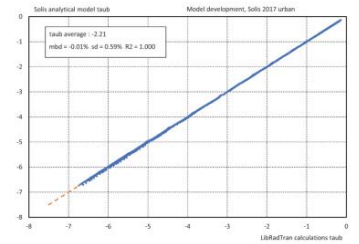

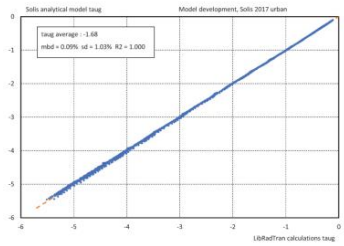

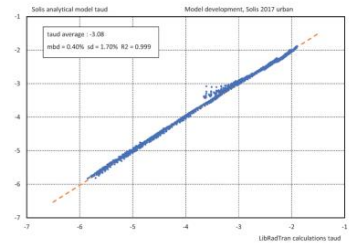

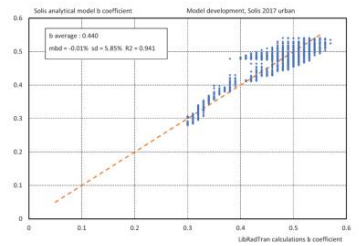

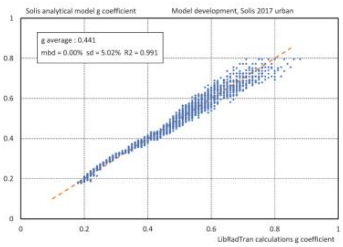

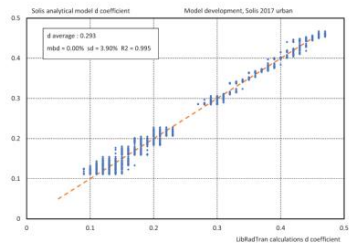

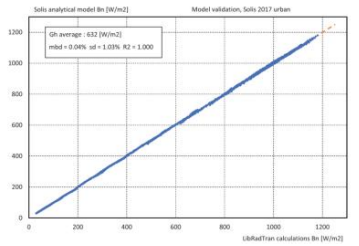

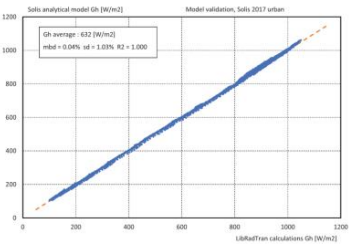

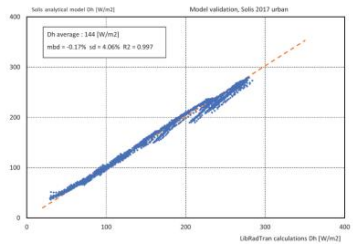

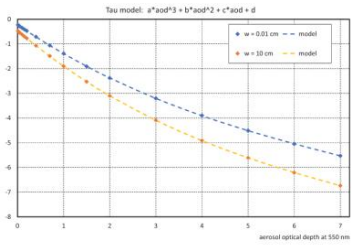

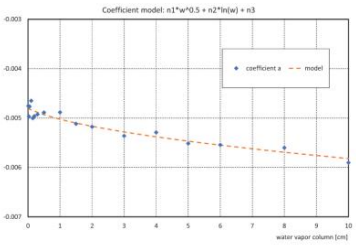

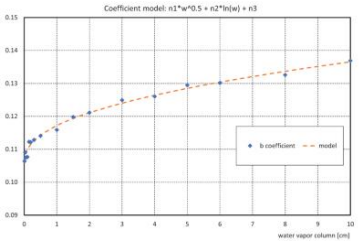

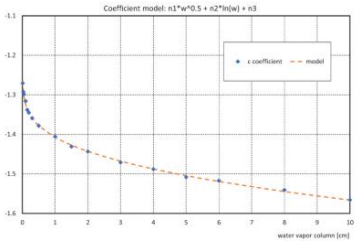

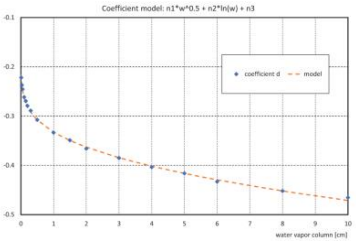

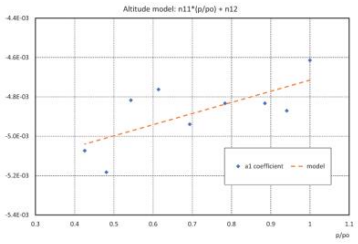
Altitude model: n11*(p/po) + n12
a1 coefficient
model
p/po

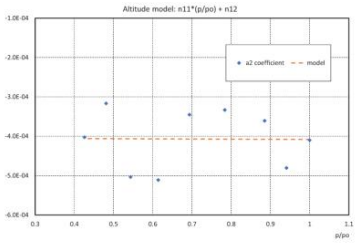
Altitude model: n11*(p/po) + n12
a2 coefficient
model
p/po

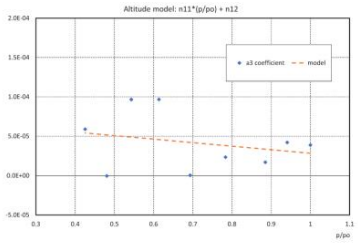
Altitude model: n11*(p/po) + n12
a3 coefficient
model
p/po

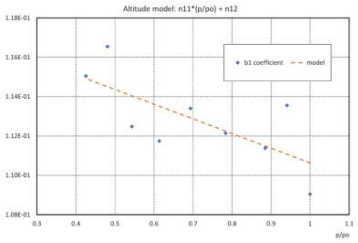
Altitude model: n11*(p/po) + n12
b1 coefficient
model
p/po

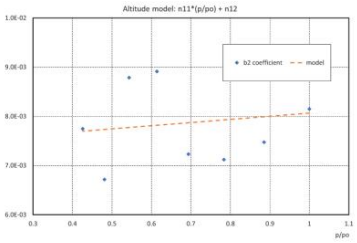
Altitude model: n11*(p/po) + n12
b2 coefficient
model
p/po

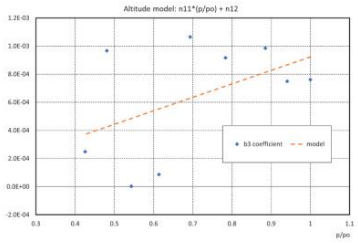
Altitude model: n11*(p/po) + n12
b3 coefficient
model
p/po

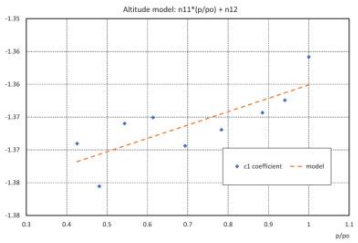
Altitude model: n11*(p/po) + n12
c1 coefficient
model
p/po

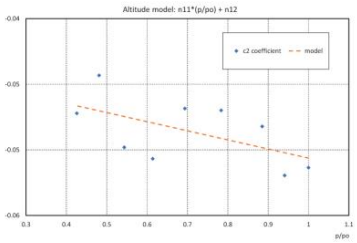
Altitude model: n11*(p/po) + n12
c2 coefficient
model
p/po

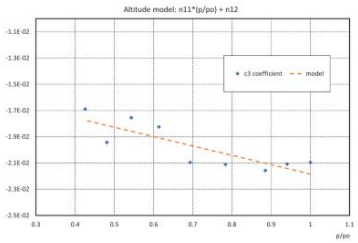
Altitude model: n11*(p/po) + n12
c3 coefficient
model
p/po

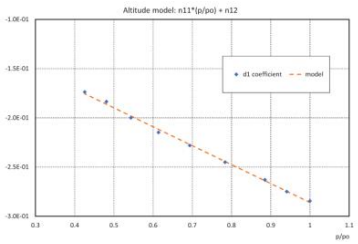
Altitude model: n11*(p/po) + n12
d1 coefficient
model
p/po

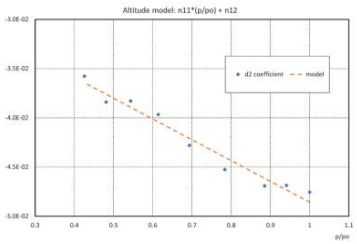
Altitude model: n11*(p/po) + n12
d2 coefficient
model
p/po

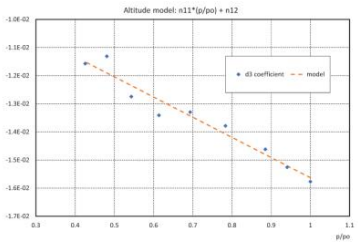
Altitude model: n11*(p/po) + n12
d3 coefficient
model
p/po